ACCOUNTS of chemical research

pubs.acs.org/accounts Article

Managing the Nitrogen Cycle via Plasmonic (Photo)Electrocatalysis: Toward Circular Economy

Mohammadreza Nazemi* and Mostafa A. El-Sayed*

Cite This: *Acc. Chem. Res.* 2021, 54, 4294–4304 Read Online

CONSPECTUS: As renewable energy sources are either intermittent in nature or remote in location, developing cost-effective, sustainable, modular systems and technologies to store and transport renewables at an industrial scale is imperative. Storing cheap renewable electricity into chemical bonds (i.e., chemical energy storage) could be a transformative opportunity for reliable and resilient grid energy storage. This approach enables renewables to be stored and shipped similarly to fossil fuels. Currently, the chemical industry primarily consumes fossil feedstock as an energy source, which has been the standard for over a century. A paradigm shift is required to move toward a more sustainable route for chemical synthesis by electrifying and decarbonizing the modern chemical industry. As renewable electricity costs decrease, (photo)electrosynthesis is gaining interest for synthesizing high-value and high-energy fuels and molecules in a clean, sustainable, and decentralized manner.

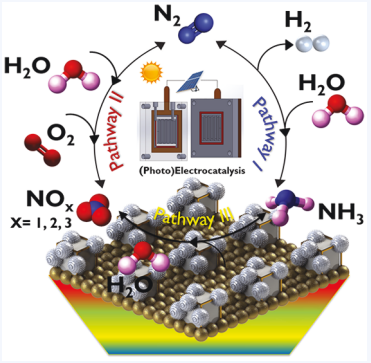

The nitrogen cycle is one of the Earth's most critical biogeochemical cycles since nitrogen is a vital element for all living organisms. Artificial nitrogen fixation via a (photo)electrochemical system powered by renewables provides an alternative route to resource- and carbon-intensive thermochemical processes. (Photo)electrochemical nitrogen fixation at a large scale necessitates the discovery of active, selective, and stable heterogeneous (photo)electrocatalysts. In addition, the use of advanced *in situ* and *operando* spectroscopic techniques is needed to pinpoint the underlying reaction mechanisms. The selectivity of nitrogen (N_2) molecules on the catalyst surface and suppressing thermodynamically favorable side reactions (e.g., hydrogen evolution reaction) are the main bottlenecks in improving the rate of (photo)electrochemical nitrogen fixation in aqueous solutions. The rational design of electrode, electrolyte, and reactors is required to weaken the strong nitrogen−nitrogen triple bond (N≡N) at or near ambient conditions. This Account covers our group's recent advances in synthesizing shape-controlled hybrid plasmonic nanoparticles, including plasmonic−semiconductor and plasmonic−transition metal nanostructures with increased surface areas. The nanocatalysts' selectivity and activity toward nitrogen conversion are benchmarked in liquid- and gas-phase electrochemical systems. We leverage *operando* vibrational-type spectroscopy (i.e., surface-enhanced Raman spectroscopy (SERS)) to identify intermediate species relevant to nitrogen fixation at the electrode−electrolyte interface to gain mechanistic insights into reaction mechanisms, leading to the discovery of more efficient catalysts. *Operando* SERS revealed that the nitrogen reduction reaction (NRR) to ammonia on hybrid plasmonic−transition metal nanoparticle surfaces (e.g., Pd−Ag) occurs through an associative mechanism. In the NRR process, hydrazine (N_2H_4) is consumed as an intermediate species. A femtosecond pulsed laser is used to synthesize hybrid plasmonic photocatalysts with homogeneously distributed Pd atoms on a Au nanorod surface, resulting in enhanced optoelectronic and catalytic properties. The overarching goal is to develop modular photoelectrochemical systems for long-duration renewable energy storage. In the context of nitrogen fixation, we aim to propose strategies to manage the nitrogen cycle through the interconversion of N_2 and active nitrogen-containing compounds (e.g., NH_3, NO_x), enabling a circular nitrogen economy with sustainable and positive social and economic outcomes. The versatile approaches presented in this Account can inform future opportunities in (photo)electrochemical energy conversion systems and solar fuel-based applications.

KEY REFERENCES

- Nazemi, M.; Panikkanvalappil, S. R.; El-Sayed, M. A. Enhancing the rate of electrochemical nitrogen reduction reaction for ammonia synthesis under ambient conditions using hollow gold nanocages. *Nano Energy* **2018**, *49*, 316−323.[1] *Electrochemical nitrogen reduction reaction (NRR) was demonstrated using Au nanoparticles of various shapes and types. The 3-fold enhancement in NRR Faradaic*

Received: July 21, 2021
Published: November 1, 2021

https://doi.org/10.1021/acs.accounts.1c00446
Acc. Chem. Res. 2021, 54, 4294−4304

efficiency is achieved using hollow Au nanoparticles compared to solid counterparts.

- Nazemi, M.; El-Sayed, M. A. Plasmon-enhanced photo (electro) chemical nitrogen fixation under ambient conditions using visible light responsive hybrid hollow Au-Ag_2O nanocages. *Nano Energy* **2019**, *63*, 103886.[2] *The coupling of the plasmonic enhancement of Au nanocages with a visible-light active p-type semiconductor enhances the photocatalytic NRR activity. No sacrificial reagent was used to drive photochemical redox reactions.*
- Nazemi, M.; Ou, P.; Alabbady, A.; Soule, L.; Liu, A.; Song, J.; Sulchek, T. A.; Liu, M.; El-Sayed, M. A. Electrosynthesis of Ammonia Using Porous Bimetallic Pd−Ag Nanocatalysts in Liquid-and Gas-Phase Systems. *ACS Catal.* **2020**, *10*, 10197−10206.[3] *We demonstrate electrochemical ammonia synthesis in liquid- and gas-phase systems at current densities exceeding 1 mA* cm^{-2}. *Operando surface-enhanced Raman spectroscopy (SERS) and density functional theory (DFT) were leveraged to probe the reaction mechanism.*
- Nazemi, M.; Panikkanvalappil, S. R.; Liao, C.-K.; Mahmoud, M. A.; El-Sayed, M. A. Role of Femtosecond Pulsed Laser-Induced Atomic Redistribution in Bimetallic Au−Pd Nanorods on Optoelectronic and Catalytic Properties. *ACS Nano* **2021**, *15*, 10241−10252.[4] *We showed that femtosecond pulsed laser-induced atomic redistribution of Pd in bimetallic Au−Pd nanorods (NRs) resulted in enhanced optoelectronic and catalytic properties of hybrid plasmonic−catalytic nanoparticles.*

1. INTRODUCTION

Storing cheap renewable electricity into chemical bonds (i.e., electrons to fuels) can offer an attractive method for long-duration energy storage to address the intermittency of renewables and balance the mismatch between renewable energy supply and demand at the grid.[5,6] This approach enables the electrification and decarbonization of the commodity chemicals industry, which has been heavily dependent on fossil fuels. A transition from carbon-based fuels to carbon-free fuels must consider the environmental and social impacts caused by the production and consumption of these new fuels and chemicals. The nitrogen cycle is one of the most critical biogeochemical cycles on Earth since nitrogen is an essential nutrient for sustaining all forms of life, including bacteria, plants, and humans.[7] In nature, different nitrogen-containing compounds are interconverted at a scale of million metric tons per year.[7] The air in the Earth's atmosphere is comprised of approximately 78% gaseous nitrogen (N_2). N_2 can be used by living organisms in its reactive form (e.g., ammonia). Natural or biological N_2 fixation occurs through the enzyme nitrogenase, resulting in 120 million metric tons of fixed N_2 available to the biosphere.[8] The nitrogenase enzyme, the widely studied one that contains iron and molybdenum (FeMo nitrogenase), is responsible for catalyzing the N_2 reduction reaction (NRR) to ammonia at mild conditions (<40 °C, atmospheric pressure).[9,10] Artificial fixation of N_2 into ammonia (NH_3), nitric acid (HNO_3), hydrazine (N_2H_4), and other valuable nitrogen-containing species is key to the nitrogen economy. Artificial N_2 fixation predominantly occurs through the thermochemical process (i.e., Haber−Bosch). This process produces 180 million metric tons of ammonia annually and is responsible for feeding nearly half of the world's population.[11,12] In the Haber−Bosch reactor, hydrogen and nitrogen react on a heterogeneous catalyst made of iron (Fe) at well above atmospheric pressures and temperatures. This process accounts for more than 1% of global energy consumption and emits 1.2% of global CO_2.[13] Nitric acid is almost entirely produced by oxidizing ammonia through the Ostwald process. In addition, nitrogen oxide (NO) formation in N_2 and O_2 atmosphere takes place at high temperatures (>2000 °C). Both approaches take place through thermal catalysis with a significant carbon footprint.[6] Electrification of ammonia synthesis enables the long-term storage of renewable energy in the ammonia chemical bonds. The stored energy in the form of liquid fuel can be transported and delivered to end-users for various applications in the energy, agricultural, and transportation industries.[14−16]

Various (photo)electrically driven strategies have been proposed to activate and cleave N≡N at or near ambient conditions, including direct N_2 electrolysis, a Li-mediated approach, and plasma-enabled N_2 fixation. Depending on the adsorption and protonation modes of N_2, the activation mechanisms are classified into associative and dissociative pathways. In the associative mechanisms, the N≡N cleavage and protonation occur simultaneously, while in the dissociative pathways, the N≡N triple bond is broken before protonation.[17,18] (Photo)electrochemical approaches are potentially promising to manage the nitrogen cycle through the interconversion of N_2 and water (hydrogen and oxygen source) to nitrogen-containing fuels and fertilizers. This is accomplished by integrating a renewably derived electricity system (e.g., photovoltaic (PV) or wind) to an electrochemical cell or by designing a single photoelectrochemical (PEC) device.[19,20] The development of sustainable and stable aqueous and biosourced solar cells to power an electrochemical system makes this approach more appealing for further discovery.[21,22] The main challenge associated with (photo)electrocatalytic N_2 fixation is the low selectivity and activity toward desired molecules (i.e., low Faradaic and energy efficiencies) and the short durability of catalyst materials. This mandates developing a strategy to boost the desired reaction interface kinetics and create suppression mechanisms for unwanted products to obtain superior performances. In the Li-mediated method, Li reacts with N_2 at room temperature to generate lithium nitride (Li_3N). Then, the reaction of Li_3N with proton sources present in the electrolyte forms ammonia.[23−25] In plasma-catalytic nitrogen fixation, the collision of N_2 with plasma-generated highly energetic electrons generates vibrationally excited nitrogen species (N_2*). Then, the reaction between N_2* and oxygen or hydrogen radicals (in the gas phase or water) produces ammonia or nitrogen oxides.[26,27] While the Li-mediated approach and plasma catalysis are promising in achieving high product yield and Faradaic efficiency, future work must focus on devising strategies to improve energy efficiency.

In this Account, we discuss our group's recent advances in designing and synthesizing shape-controlled hybrid plasmonic nanoparticles as (photo)electrocatalysts and their applications in (photo)electrochemical systems. *Operando* surface-enhanced Raman spectroscopy (SERS) provides insights into chemical transformations at the electrode−electrolyte interfaces to pinpoint underlying mechanisms in catalysis. A femtosecond pulsed laser is used to discover hybrid plasmonic−transition metal photocatalysts with enhanced optoelectronic and catalytic properties. We combined materials chemistry, photoelectrochemistry, and spectroscopy to understand plasmonic (photo)-

https://doi.org/10.1021/acs.accounts.1c00446
Acc. Chem. Res. 2021, 54, 4294−4304

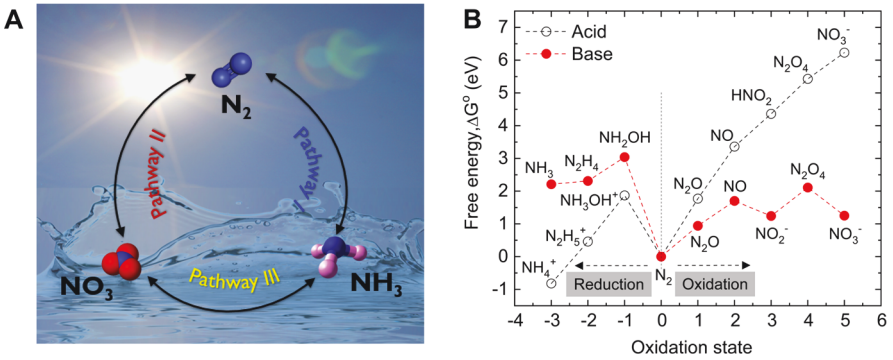

Figure 1. (A) Various routes for interconversion of nitrogen and nitrogen-containing compounds to enable a circular nitrogen economy. (B) Free energy diagram for nitrogen oxidation and reduction states in acidic and basic solutions. Data from ref 28.

electrocatalysis to develop next-generation technologies with broad applications for distributed chemical synthesis.

2. CLOSING THE NITROGEN CYCLE

Redox chemistry of N_2 consists of compounds with nitrogen oxidation states ranging from −3 (NH_3) to +5 (NO_3^-).[28] In the nitrogen cycle, N_2 with an oxidation state of zero can be converted (i.e., reduced) to ammonia (oxidation state = −3) using H^+ or H_2O (pathway I in Figure 1A) to balance the half-cell reaction in eq 1:

$$N_2(g) + 6H^+ + 6e^- \rightarrow 2NH_3(g)$$
$$E^\circ = 0.057 \text{ V vs RHE} \quad (1)$$

The overall reaction assuming water oxidation (1.23 V vs RHE) at the anodic compartment is given by eq 2:

$$N_2(g) + 3H_2O(l) \rightarrow 2NH_3(g) + \frac{3}{2}O_2(g)$$
$$E^\circ = 1.17 \text{ V vs RHE} \quad (2)$$

Ammonia oxidation is also a major step in global nitrogen cycling. Ammonia is a multipurpose chemical due to the existence of N and H elements in its structure. The N element makes the compound a valuable agrochemical, while the H element enables ammonia oxidation ($NH_3 \rightarrow \frac{1}{2}N_2 + \frac{3}{2}H_2$) to be utilized in clean energy sectors, such as transportation and electricity storage and generation. N_2 fixation can also occur through the oxidative pathway with either O_2 or H_2O to produce NO_x (x = 1, 2, 3) with the oxidation states of +2, +3, and +5 (pathway II in Figure 1A), which are also vital chemical feedstocks for agrochemical and pharmaceutical products. Currently, NO_x is primarily produced via ammonia oxidation in the thermocatalytic process. Direct electrochemical nitrogen oxidation reaction (NOR) to generate nitrate (eq 3) could be more appealing, which also does not require NH_3 as an intermediate agent.

$$N_2(g) + 6H_2O \rightarrow 2NO_3^-(aq) + 12H^+ + 10e^-$$
$$E^\circ = 1.076 \text{ V vs RHE} \quad (3)$$

According to eq 3, NOR is thermodynamically more favorable than the competing side oxygen evolution reaction (1.23 V vs RHE). Therefore, one might consider coupling NOR at the anode with NRR at the cathode (eq 1) in a full electrochemical cell with a minimum theoretical potential of ∼1.02 V.[29]

The environmental consequences due to the overuse of nitrogen-based fertilizers include surface and groundwater nitrate (NO_3^-) pollution from fertilizer runoff, eutrophication of freshwater systems, and massive killing of aquatic organisms in coastal regions that comprise so-called "dead zones" due to depleted oxygen. Reduction of NO_3^- to NH_3 (pathway III in Figure 1A) can occur according to the following reaction:

$$NO_3^-(aq) + 6H_2O + 8e^- \rightarrow NH_3(g) + 9OH^-$$
$$E^\circ = 0.7 \text{ V vs RHE} \quad (4)$$

The conversion of NO_3^- to NH_3 will have positive environmental impacts through wastewater treatment and also paves the way for nutrient recovery and recycling.[30−32] Developing (photo)electrocatalytic approaches for interconversion of N_2 and active nitrogen-based compounds (e.g., NO_x, NH_3) will enable a circular nitrogen economy, mitigate waste, and promote sustainability. As the free energy for all intermediate nitrogen oxidation states is pH-dependent, it is imperative to control the catalyst microenvironment (e.g., local proton activity) to direct reactivity along desired pathways (Figure 1B). The free energy (ΔG°) is given by the following equation:

$$\Delta G^\circ = -nF\Delta E^\circ \quad (5)$$

where n is the number of electrons required in an electrochemical reaction, F is Faraday's constant (96 485 C/mol) and ΔE° is the potential for the half-cell reaction. Here, the nitrogen oxidation state (i.e., zero) is used as the reference point, and it is assumed that all other nitrogen-based species are formed from N_2, electrons, H^+ or OH^-, water, and other species. The free energy change for ammonia formation is lower in acidic solution (pH = 0) than in basic solution (pH = 14). Ammonia formed in acidic solution primarily exists as ammonium ions (NH_4^+) dissolved in the electrolyte. Hydrogen evolution reaction (HER) is the competing side reaction in acidic media. NO_3^- formation requires significantly lower ΔG° under basic conditions than acidic ones (Figure 1B).

3. NANOCATALYSIS WITH HYBRID PLASMONIC NANOPARTICLES

Nanoparticles are characterized by a high surface-to-volume ratio, enhancing efficiency in homogeneous and heterogeneous catalytic reactions.[33] Hollow nanocatalysts are particularly attractive due to the higher surface area than their solid counterparts and the confinement of reactants within the cavity (cage effect). The galvanic replacement technique was developed to synthesize hollow metallic nanoparticles of various shapes and sizes.[34] In this technique, the sacrificial metal template (e.g., silver) with a higher oxidation potential is

https://doi.org/10.1021/acs.accounts.1c00446
Acc. Chem. Res. 2021, 54, 4294−4304

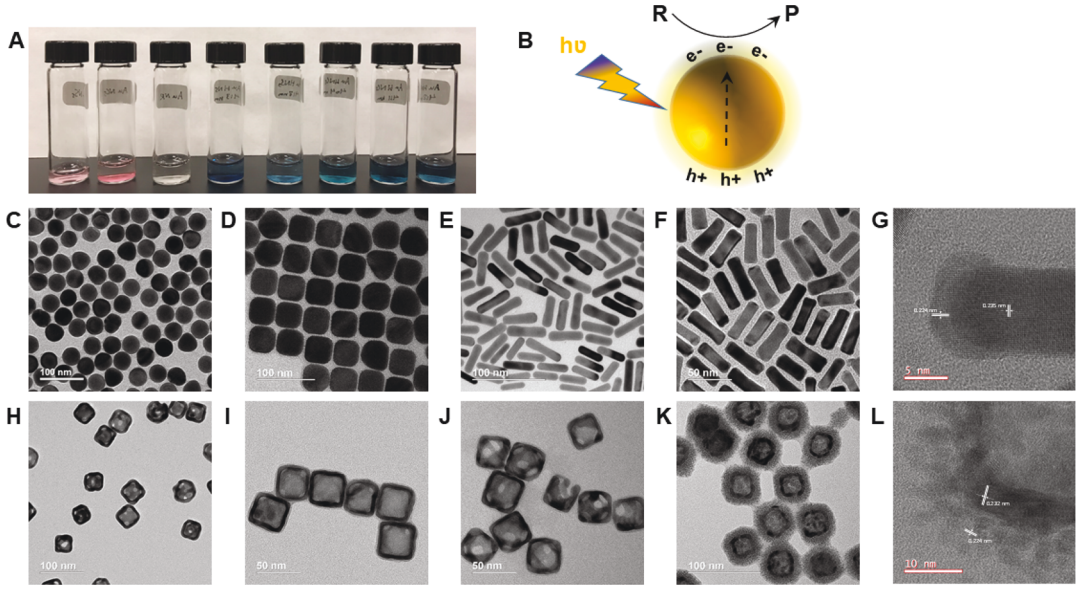

Figure 2. (A) Colloidal plasmonic nanoparticles of various types (solid and hollow) and shapes (spheres, cubes, rods). (B) Excitation of a plasmonic nanoparticle with incident light, resulting in generation of an electromagnetic field, hot holes, and hot electrons for chemical transformations. TEM images of single plasmonic metal, bimetallic, trimetallic, and semiconductor−plasmonic nanoparticles, including (C) gold nanospheres (AuNSs), (D) gold nanocubes (AuNCs), (E) gold nanorods (AuNRs), and (F) gold−palladium nanorods (AuPdNRs), and (G) high-resolution TEM (HRTEM) image of AuPdNRs revealing lattice spacings of 0.235 and 0.224 nm, which correspond to face-centered cubic (FCC) structure Au and Pd. TEM images of (H) hollow gold nanocages (AuHNCs), (I, J) gold−silver(I) oxide (Au−Ag_2O) with different pore sizes, and (K) gold−silver−palladium nanoparticles (Au−Ag−Pd) and (L) HRTEM image of Pd−Ag nanocages showing lattice spacings of 0.232 and 0.224 nm, corresponding to the (111) lattice plane of the FCC structure Ag and Pd. Panels C−E and H were reproduced with permission from ref 1. Copyright 2018 Elsevier. Panels F and G were reproduced with permission from ref 4. Copyright 2021 American Chemical Society. Panels I and J were reproduced from ref 2. Copyright 2019 Elsevier. Panel K was reproduced with permission from ref 55. Panel L was reproduced with permission from ref 3. Copyright 2020 American Chemical Society.

replaced with the nanocage metal (e.g., gold). By replacing three Ag atoms from the template with one Au atom, a hollow structure is created with holes at the wall and corners of the nanocages. The size and shape of the resulting nanocage metals can be engineered by changing the size and shape of the metal template. Confinement of reactants within the hollow nanocatalysts has been shown to enhance the catalytic efficiency of various chemical reactions by comparing the catalytic activity of gold nanocages with that of the solid nanocatalysts of various shapes (Figure 2).[1,35] In particular, electrochemical NRR was demonstrated using hollow Au nanocages (AuHNCs) as an electrocatalyst with three times higher ammonia Faradaic efficiency than that of solid Au nanocubes (AuNCs).[1] In addition, the pore size should be optimized so that reactants can diffuse in and products can diffuse out of the cavity while not reducing the surface area considerably due to the increase in the pore size in the walls and corners of the nanocages. We demonstrated that AuHNCs with localized surface plasmon resonance (LSPR) peak position at 715 nm with average edge length of 40 nm, shell thickness of 4 nm, and pore sizes of 8 nm at the walls and corners are the most efficient nanocatalysts to maximize the cage effect.[36,37]

Noble metal nanoparticles that are characterized by localized surface plasmon resonance (LSPR), commonly known as plasmonic nanoparticles, support coherent oscillatory modes of their conduction band electrons when photoexcited with a resonant frequency. This generates a strong electromagnetic field near the nanoparticle surface, excited hot carriers, and photothermal heating. In redox reactions that involve electron transfer steps, hot electron−hole pairs generated by plasmonic excitation are the primary driving force for chemical transformations, and photothermal heating that can be as high as 10 °C depending upon the light power intensity (0−3 W cm^{-2}) has a negligible effect on the rate of the reaction.[38,39] The LSPR can be excited by ultraviolet (UV), visible, or near-infrared (NIR) light depending on the size, shape, composition, structure, and dielectric function of the surrounding medium. In addition, by coupling the electromagnetic fields generated by individual plasmonic nanoparticles, a stronger electromagnetic field can be generated, depending upon the orientation and the number of adjacent nanoparticles on the substrate.

The plasmonic excitation of metal nanoparticles generates nonthermal hot electrons on a few femtosecond time scale through electron-surface scattering. These hot electrons can excite electronic or vibrational transitions in adsorbed species on nanoparticles surfaces, enabling catalytic reactions. Plasmonic nanoparticles have shown moderate catalytic activity for driving chemical reactions. Various strategies, including incorporating a transition metal catalyst or a semiconductor shell, have been proposed to enhance plasmonic nanocatalyst (photo)-electrocatalytic activity.[2,4] In the hybrid plasmonic−transition metal catalysts, a plasmonic nanoparticle primarily absorbs light and generates hot holes and electrons, while a transition metal cocatalyst handles the chemical transformations. Plasmonic nanoparticles can also act as sole catalysts, which has been demonstrated for the CO_2 reduction reaction.[40] It is noted that to avoid the masking effect due to the blocking of the light by plasmonic catalysts on the front layer, these catalysts are distributed on a substrate with a suitable surface area so that this effect is minimal.[3] In our reported studies, SEM images confirm that we form a monolayer of plasmonic nanoparticles to minimize the masking effect.[3,4]

https://doi.org/10.1021/acs.accounts.1c00446
Acc. Chem. Res. 2021, 54, 4294−4304

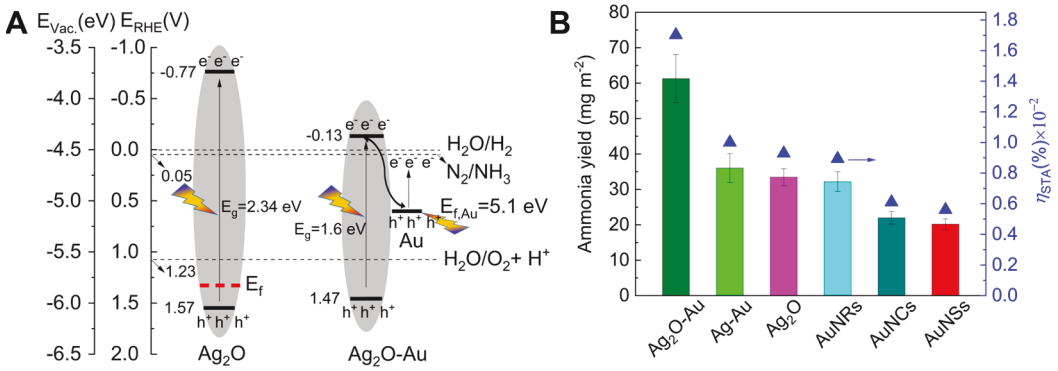

Figure 3. (A) Electronic band structure of Ag_2O and Ag_2O−Au photocatalysts for NRR. The electronic band structures of Ag_2O and Ag_2O−Au are determined through optical band gaps and ultraviolet photoelectron spectroscopy (UPS) measurements. The position of the valence band maximum (E_{VBM}) is determined by summing the valence band offset at low binding energy ($E_F - E_{VBM}$) and the secondary electron onset, which is referenced to the 21.21 eV helium source energy ($E_{VAC} - E_F$). The UV−vis spectra of photocatalysts are analyzed by the Kubelka−Munk theory to determine the optical band gap. (B) Ammonia yield and solar-to-ammonia efficiency (η_{STA}) of various photocatalysts under one sun illumination in a N_2-saturated pure water system. Reproduced with permission from ref 2. Copyright 2019 Elsevier.

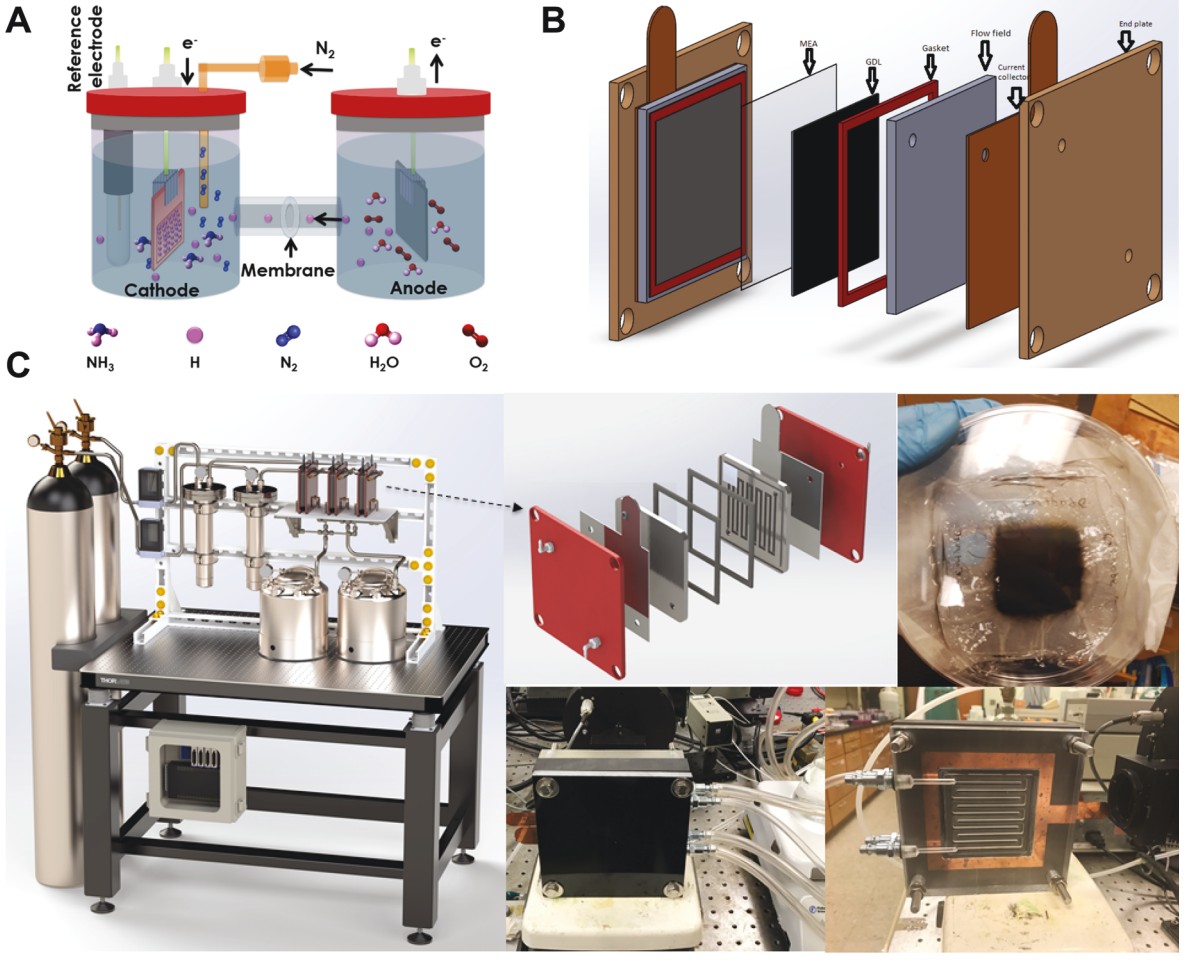

Figure 4. (A) Schematic diagram of liquid-phase (H-cell) electrochemical cell for NRR. A proton exchange membrane separates anode and cathode compartments. Protons generated by water oxidation at the anode are transferred across the membrane to the cathode where NRR occurs. Reproduced with permission from ref 1. Copyright 2018 Elsevier. (B) Schematic illustration of the MEA-type cell for gas-phase electrochemical nitrogen fixation for ammonia synthesis. The cell consists of a catalyst-coated membrane, gas diffusion layers, current collectors and end plates. Reproduced with permission from ref 3. Copyright 2020 American Chemical Society. (C) Schematic of the gas-phase photoelectrochemical cell for nitrogen fixation under visible-light illumination using hybrid photoelectrocatalysts developed in El-Sayed's lab. In this setup, the flow field and gas diffusion layer are combined in a single component (i.e., transparent end plate), allowing the exposure of the photoelectrocatalyst to the incident light. The catalyst materials are painted on both sides of the membrane surface, as shown in the top right image. Note that the generated ammonia in the gas form will be liquefied using the condenser as depicted on the benchtop.

https://doi.org/10.1021/acs.accounts.1c00446
Acc. Chem. Res. 2021, 54, 4294−4304

In the hybrid plasmonic−semiconductor nanoparticles, a visible-light responsive semiconductor can be coupled with a plasmonic metal to achieve higher (photo)electrocatalytic activity. This is accomplished by increasing the number of photogenerated charge carriers upon visible light illumination.[2] By oxygenating hollow bimetallic Au−Ag nanocages with pure oxygen gas, Ag is oxidized to Ag_2O without affecting the shape and the pore size of the resulting nanoparticles (Figure 2I,J). Ag_2O is a highly stable p-type semiconductor under ambient conditions. As the work function ($\varnothing$) of the Ag_2O is higher than that of the Au plasmonic metal ($\varnothing_s > \varnothing_m = 5.1$ eV), a Schottky barrier is formed at the metal−semiconductor interface, where photogenerated holes are transferred from Ag_2O to Au, so that the Fermi levels in the metal and semiconductor are matched.[2] Valence and conduction bands in the semiconductor bend downward to match the chemical potentials. The photogenerated electron transfer from the Ag_2O conduction band to the Au plasmonic metal surface can occur, or hot electrons generated by Au can be injected into the Ag_2O conduction band. These electron transfer processes are possible and sometimes competitive, which might improve or deteriorate the photocatalytic reaction rate. In addition, photoluminescence (PL) measurements revealed that the emission intensity for Ag_2O−Au is significantly lower than that of the pure Ag_2O, suggesting fluorescence quenching by the Au nanoparticles.[2] The electronic structures of Ag_2O and Ag_2O−Au revealed that both photocatalysts are active under visible light illumination. In addition, the valence band maximum (E_{VBM}) and conduction band minimum (E_{CBM}) energy levels indicate that photocatalysts can drive water oxidation reaction and NRR through photogenerated holes and electrons without the need for the sacrificial reagent (Figure 3A). The highest photocatalytic NRR activity is achieved for the hybrid plasmonic−semiconductor (i.e., Ag_2O−Au nanocages), attributed to the combined effects of hot electrons generated by Au nanoparticles and photogenerated electrons by the semiconductor (Figure 3B). The amount of ammonia formation under visible light irradiation (47.8 mg m^{-2}) and on-plasmon resonance excitation (39.11 mg m^{-2}) using a monochromatic light source highlights the critical role of the plasmonic excitation effect. This indicates that the off-plasmon resonance has a small contribution to the overall ammonia formation, which can stimulate the Ag_2O semiconductor.[2]

4. (PHOTO)ELECTROCHEMICAL REACTOR DESIGN

Designing and integrating system components into a single catalytic reactor is critical for the selective, efficient, and durable production of fuels and chemicals. Reactor designs are typically divided into three main categories: single-chamber cell, double chamber cell (H-type cell), and membrane electrode assembly (MEA)-type cell. Various cell designs can be adopted for (photo)electrochemical nitrogen fixation that are differentiated by catalyst materials, membranes, electrolytes, and reaction parameters (e.g., temperature and pressure).[41]

In single-compartment systems, oxidation and reduction occur in the same cell, leading to potential diffusion and oxidation of ammonia at the anode. Separating the anodic and cathodic reactions is an effective route to address this limitation of single-compartment cells. In double-chamber cells or H-type cells, anodic and cathodic compartments are separated by cation or anion exchange membranes, allowing the transport of H^+ and OH^- ions across the membrane to balance the redox reactions (Figure 4A). The majority of the produced NH_3 is in the form of ammonium (NH_4^+) in aqueous electrolytes, which cannot transport across the membrane, preventing the oxidation and loss of ammonia as compared to single-chamber cells. Therefore, it is essential to choose suitable membranes to minimize the product crossover and measure the total ammonium concentration in both anodic and cathodic chambers. A portion of products may still transfer through the membrane to the anode chamber. Note that extensive control experiments should be carried out, including isotopic labeling experiments using $^{15}N_2$ gas to avoid false-positive ammonia formation by various sources of impurities and contamination.[42−44] $^{15}N_2$ (98 atom % ^{15}N) should be purified before use in experiments by passing through an absorber (e.g., 1 mM H_2SO_4) followed by deionized water to remove trace amounts of NO_x and NH_3 present in the feed gas. In addition, as the membrane, especially bipolar membranes, avoids species crossover, the electrolytes in the two compartments can be different. This provides an opportunity to optimize redox reaction environments.

In the membrane-electrode assembly type (MEA-type) reactors, N_2 and H_2 or water vapor are directly fed into the system. The redox reactions occur at the intersection where the gaseous reactant, electron-conducting catalyst, and ion-conducting membrane meet (Figure 4B).[3,45,46] This apparatus enables overcoming the transport limitation due to the low solubility of N_2 in the aqueous electrolyte. Note that the concentration of N_2 in the gas phase is about 140× higher than the saturation concentration of dissolved N_2 in the aqueous electrolyte. Our recent report demonstrated that the energy efficiency of the gas-phase system can be ∼3× higher than that of the liquid-phase one under the same operating current density, primarily due to the decrease in ohmic losses by elimination of the liquid electrolyte.[3] In addition, the gas-phase system allows us to produce desired chemicals with little to no additional steps for separation and purification.

Combining catalysts with light-harvesting materials in electrochemical systems leads to photoelectrochemical (PEC) cells. A typical PEC cell consists of a light source, a reaction cell, and a three-electrode system. PEC N_2 reduction occurs using a photocathode at the working electrode, and the water oxidation reaction occurs at the counter electrode (dark anode). The PEC systems can be either single-chamber cells or H-cells.[47,48] A gas-phase PEC system is developed by combining the flow field and the gas diffusion layer into a single component (transparent end plate), allowing the transmission (>95%) of the incident light through the end plate to reach the photoelectrocatalyst (Figure 4C). The anodic part of the cell is similar to the MEA-type electrochemical cells. For the oxidative pathway, a photoanode for N_2 oxidation will be coupled with a dark cathode to balance the photoredox reactions. In addition, the stability of nanostructured electrodes is evaluated by conducting consecutive cycles for a certain test period (e.g., 12 h). Postcharacterization of nanoparticles is carried out via electron microscopy and advanced spectroscopy techniques to determine the morphological changes, oxidation states, and electronic structure of materials.[3,4]

5. DESIGN OF HYBRID PLASMONIC PHOTOCATALYSTS VIA FEMTOSECOND PULSED LASER

Incorporating transition metal cocatalysts into plasmonic nanoparticles can improve catalytic activity. The exposure of hybrid plasmonic−transition metal nanocatalysts to a femto-

https://doi.org/10.1021/acs.accounts.1c00446
Acc. Chem. Res. 2021, 54, 4294−4304

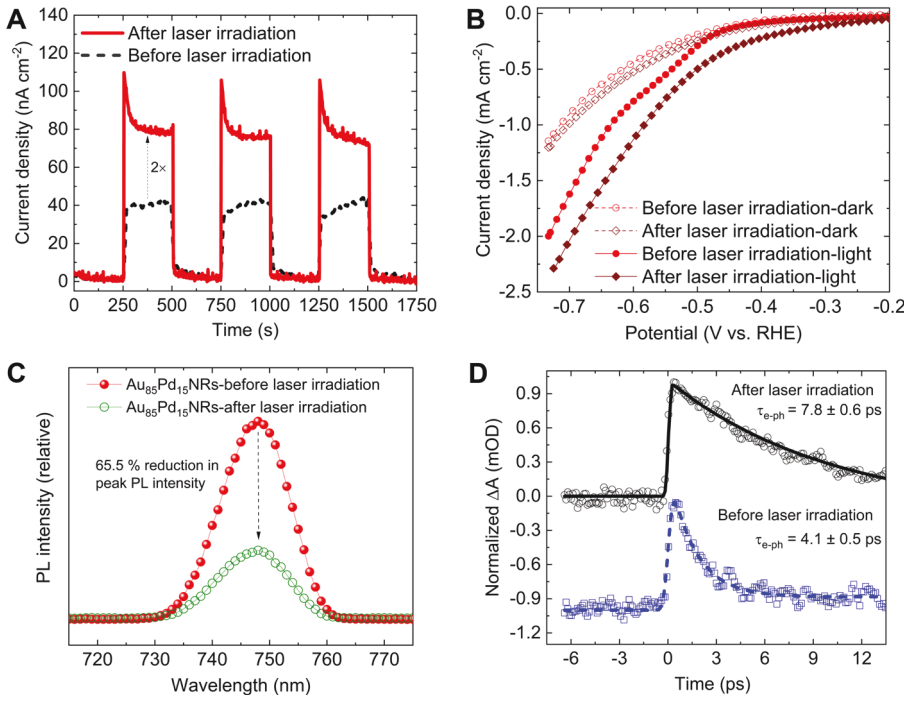

Figure 5. (A) Transient photocurrent response of AuPdNRs before and after femtosecond pulsed laser-induced atomic redistribution (808 nm laser source, 200 mW). (B) LSV of AuPdNRs before and after laser-induced reshaping under dark and light conditions. (C) PL spectra of AuPdNRs before and after femtosecond laser irradiation. The peak PL intensity decreases after surface modification of AuPdNRs via femtosecond laser irradiation, suggesting more effective quenching of hot carriers by Pd sites. (D) Kinetic traces from TA spectra for plasmon bleach recovery of AuPdNRs before and after femtosecond laser irradiation pumped at 405 nm and probed at 510 nm for transverse surface plasmon absorption of nanoparticles. The black solid and blue dashed lines are fitted to experimental data with decay times of 4.1 ± 0.5 ps and 7.8 ± 0.6 ps for electron−phonon coupling times (τ_{e-ph}). Reproduced with permission from ref 4. Copyright 2021 American Chemical Society.

second pulsed laser manipulates the structure. It also induces atomic redistribution, resulting in the discovery of nanostructures with modified optoelectronic and catalytic properties.[49−51] As atomic redistribution in a hybrid nanostructure affects the catalytic performance, femtosecond pulsed laser irradiation enables modification of catalytically active sites by structural reorganization of atomic species within hybrid nanoparticles. Bimetallic AuPdNRs are synthesized through the reduction of palladium salt on the AuNR surface. Pd atoms are primarily accumulated at the tip of AuNRs.[4] Femtosecond laser irradiation of AuPdNRs with 40 fs pulse duration centered at 808 nm uniformly distributed Pd atoms with an average size of 1.5−2 nm on the AuNR surface. A slight shape change from rods to dumbbell shapes is observed after laser irradiation.[4] The photothermal−near-field ablation hybrid mechanisms are the primary mechanism for atomic redistribution of Pd, where there is no sign of alloy formation after irradiation.[52]

The photocurrent density is increased by 2-fold after femtosecond pulsed laser irradiation of AuPdNRs, suggesting improved charge transfer kinetics at the solid−liquid interface after Pd atom redistribution on the AuNR surface (Figure 5A). In addition, the $J-V$ plot revealed that the current density under dark conditions did not change significantly before and after femtosecond pulsed laser irradiation. However, the photocurrent density under 1 sun illumination is increased tangibly in a wide range of negative bias using atomically redistributed Pd in AuPdNRs by femtosecond laser (Figure 5B). The PL spectrum of hybrid plasmonic nanoparticles shows a 65.5% reduction in emission intensity after femtosecond laser irradiation, indicating that Pd atom redistribution on the AuNR surface effectively decreases the number of hot carriers for radiative recombination, resulting in an enhanced photocurrent response (Figure 5C). Furthermore, transient absorption (TA) measurements show that the average electron−phonon coupling time (τ_{e-ph}) of bimetallic AuPdNRs increases (7.8 ± 0.6 ps) after femtosecond pulsed laser-induced atomic redistribution. This indicates the efficient transfer of hot electrons from Au to Pd sites that retards charge carrier recombination (Figure 5D). The τ_{e-ph} of Au nanoparticles of different shapes varies from 1 to 4 ps.[53] This technique informs the design and synthesis of hybrid plasmonic photocatalysts with longer electron−hole recombination that can facilitate the rate of catalytic reactions.

6. *OPERANDO* SURFACE-ENHANCED RAMAN SPECTROSCOPY

Operando surface-enhanced Raman spectroscopy (SERS) is a technique that is best suited to gain unprecedented insight into the solid−liquid interaction at the electrode−electrolyte interface, which is crucial to track the intermediate species and ultimately probe the possible reaction mechanisms.[54−56] Spectroelectrochemistry is a powerful technique that combines spectroscopy and electrochemistry. A potential is applied on a SERS active substrate, which is then monitored by changes in the Raman spectrum. The prepared nanoparticles are deposited on the working electrode and used as an electrocatalyst (Figure 6A). Cyclic voltammetry (CV) measurements are conducted in the potential range of 0.97 to −0.63 V vs RHE at a scan rate of 2.5 mV s^{-1} in Ar- and N_2-saturated electrolytes to track redox reactions (Figure 6B).

The SERS spectra in N_2- and Ar-saturated $LiClO_4$(aq) electrolyte contain a Raman band located at 932 cm^{-1}, corresponding to the stretching mode of the ClO_4^- anion

https://doi.org/10.1021/acs.accounts.1c00446
Acc. Chem. Res. 2021, 54, 4294−4304

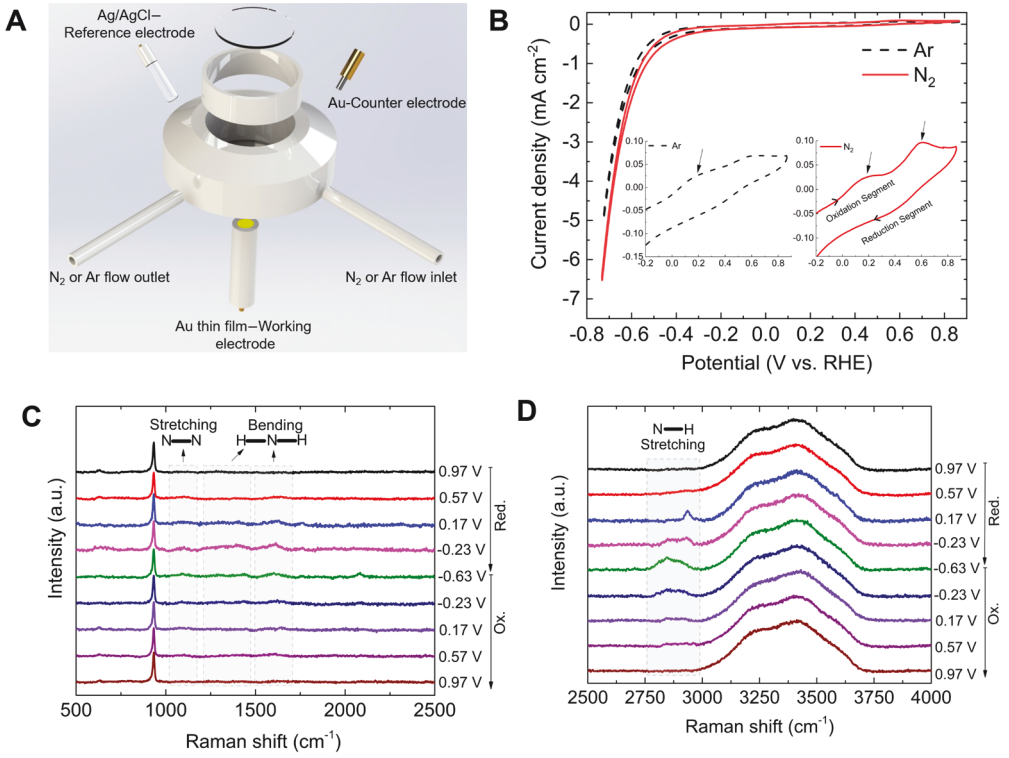

Figure 6. (A) Schematic of the spectroelectrochemical setup for *operando* SERS measurements. Reproduced with permission from ref 55. Copyright 2007 American Chemical Society. (B) CV curves of Pd–Ag nanoparticles in Ar- and N_2-saturated aqueous electrolyte at the scan rate of 2.5 mV s^{-1}. During the oxidation segment in Ar-saturated electrolyte, a strong peak centered on 0.2 V is attributed to the oxidation of hydrogen. This peak with a lower intensity is also observed in N_2-saturated electrolyte. In addition, a new peak at around 0.6 V is observed in N_2-saturated electrolyte corresponding to the oxidation of NH_3. Reprinted with permission from ref 3. Copyright 2020 American Chemical Society. (C, D) Low and high Raman shift of SERS spectra in the N_2-saturated electrolyte using Pd–Ag nanoparticles with 532 nm laser. Reproduced with permission from ref 3. Copyright 2020 American Chemical Society.

(Figure 6C). In addition, the wide vibrational band centered at 3415 cm^{-1} is attributed to O–H stretching mode due to the use of aqueous electrolyte. In addition, the SERS spectra revealed that three small peaks appear at 1101, 1394, and 1613 cm^{-1} during the reductive segment (0.97 V to −0.23 V), reaching their highest intensities at a potential of −0.23 V (Figure 6C). These peaks can be classified as N–N stretching, H–N–H scissoring, and N–H wagging, and they suggest the formation of N_2H_4 as an intermediate species during electrochemical NRR. At high Raman shift, a peak centered at 2936 cm^{-1} evolves, corresponding to the N–H asymmetric stretching mode (Figure 6D). The intensity of this peak gets stronger as we move toward more negative potentials, reaching the strongest intensity at a bias of −0.63 V. The evolution of this peak strongly supports the formation of NH_4^+ during the reductive pathway. When moving toward more negative potentials during the reductive CV scan (−0.23 V to −0.63 V), the intensity of peaks at 1094, 1393, and 1601 cm^{-1} (intermediates) decreases, while the peak at 2936 cm^{-1} reaches its highest intensity. This strongly suggests the formation of NH_3 from the intermediate species ($N_2 \rightarrow N_2H_4 \rightarrow NH_3$) (Figure 6C, D). The intensity of the peaks attributed to intermediates and ammonium decreases during the oxidative pathway due to the oxidation of the N-containing species. The SERS spectra of the standard ammonium and hydrazine solutions in 0.5 M $LiClO_4$(aq) electrolyte confirm the band assignment of various vibrational modes in *operando* SERS measurements.[3,55] Similar measurements in Ar-saturated electrolyte or without using the electrocatalyst show no noticeable peaks, indicating that the peaks are uniquely related to the generation of N-containing species.[3] Overall, *operando* SERS measurements help us to understand the reaction mechanisms to design more active and selective catalysts for (photo)electrochemical energy conversion systems.

7. FUTURE OUTLOOK

In the nitrogen cycle, ammonia is a multipurpose commodity chemical with promising opportunities to advance sustainable and renewable energy. A micro-ammonia production system (MAPS) allows for decentralized and on-site ammonia production for long-term energy storage. In the energy market, MAPS can help energy and utility companies, data centers, hospitals, etc., to store surplus electricity in the form of ammonia fuel using its chemical properties. The barrier preventing electricity producers from doing so is the lack of efficient technology to store intermittent renewables for a long duration. Therefore, MAPS can complement renewable energy and other electricity producers alike to store surplus generated energy. In addition, ammonia as a carbon-neutral energy source can be easily transported and converted back to electricity at the point of use, creating an incredibly profitable opportunity to take advantage of the arbitrage between net energy exporters with cheap electricity and net energy importers with higher electricity rates. This is because ammonia can be liquefied and stored at −33 °C and 10 bar, compared to 250 bar for liquefied natural gas (LNG) and 700 bar for liquid hydrogen. This significant reduction in storage pressure means a substantial decrease in storage tank mass and cost, thus reducing logistics cost and complexity when shipping ammonia. Furthermore, with the

https://doi.org/10.1021/acs.accounts.1c00446
Acc. Chem. Res. 2021, 54, 4294–4304

adaptation of MAPS technology to a system mirroring that of current LNG logistical networks, MAPS can be integrated into existing electrical networks, with the only additional amendments being the installation of storage tanks for the liquid ammonia and a retrofitted gas turbine or solid oxide fuel cell (SOFC) adaptor (~60% conversion efficiency). The early calculations for the energy input for ammonia electrosynthesis based on the price of renewable electricity suggest that green ammonia synthesis will be cost-competitive with the Haber–Bosch process (143 ± 14 USD) if technologies are being developed with the energy input <6 MWh_{Elec} per ton of ammonia and the price of renewable electricity is less than $0.025 per kWh (Figure 7). It is imperative to take into account

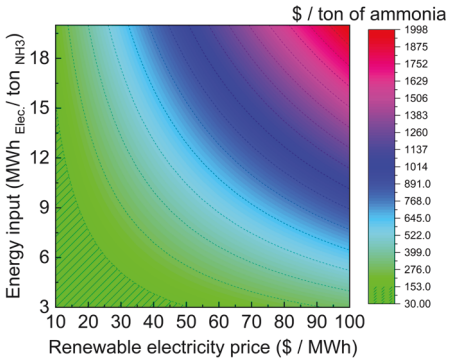

Figure 7. Input cost of green ammonia synthesis as a function of renewable electricity price and the energy input. The input cost of natural gas for making a ton of ammonia in the Haber–Bosch process is relatively constant and is about $150 (~35 314.7 ft^3 of natural gas). The hatched area is where renewable ammonia synthesis will have comparable or lower input cost than the conventional process.

the logistical price volatility of renewable electricity when considering the feasibility of this technique for commercialization. This analysis could apply to all electrified processes for ammonia synthesis, including direct electrochemical, Li-mediated, and plasma-enabled syntheses. We estimate that our MAPS is capable of producing ~165 tons of ammonia (our best performing plasmonic nanocatalyst = 23.6 mg ammonia (mg catalyst)$^{-1}$ $h^{-1}cm^{-2}$)[3] annually using a large scale electrode are (1 × 1 m^2) to satisfy our overarching goal of decentralized ammonia synthesis for energy storage and power generation sectors. This amount of ammonia is equivalent to ~858 MWh (~5.2 MWh per ton of ammonia), which is enough to power ~78 homes (average annual electricity consumption of U.S. households ≈ 11 MWh). Even though the cost of making ammonia electrochemically is currently significantly higher than the state-of-the-art Haber–Bosch process, future research should focus on improving the energy efficiency of electrochemical methods, which might find their way for some decentralized niche applications.[57]

AUTHOR INFORMATION

Corresponding Authors

Mohammadreza Nazemi − *School of Chemistry and Biochemistry, Georgia Institute of Technology, Atlanta, Georgia 30332-0400, United States;* orcid.org/0000-0002-1735-9277; Email: mrnazemi@gatech.edu

Mostafa A. El-Sayed − *School of Chemistry and Biochemistry, Georgia Institute of Technology, Atlanta, Georgia 30332-0400, United States;* orcid.org/0000-0002-7674-8424; Email: melsayed@gatech.edu

Complete contact information is available at: https://pubs.acs.org/10.1021/acs.accounts.1c00446

Notes

The authors declare the following competing financial interest(s): M.N. and M.A.E. have filed a patent application for Systems and Methods for Forming Nitrogen-Based Compounds (U.S. Patent Application 16/788,656).

Biographies

Mohammadreza Nazemi is currently a postdoctoral fellow in the School of Chemistry and Biochemistry at the Georgia Institute of Technology (Georgia Tech). He received his Ph.D. from the Woodruff School of Mechanical Engineering at Georgia Tech under the supervision of Prof. Mostafa El-Sayed in 2020. He received his M.S. degree (2015) in Mechanical Engineering from Michigan Technological University and B.S. degree (2013) in Aerospace Engineering from the Sharif University of Technology. His current research focuses on the development and testing of hybrid plasmonic nanostructures with broad applications in energy conversion and storage. In addition, he leverages advanced spectroscopic and microscopic techniques to gain a mechanistic understanding of (photo)electrochemical reactions for sustainable fuel and fertilizer production.

Mostafa A. El-Sayed is the Regents' Emeritus Professor and the director of the Laser Dynamics Laboratory in the School of Chemistry and Biochemistry at Georgia Tech. He received his B.S. from Ain Shams University in Egypt and his Ph.D. from Florida State University in 1959 with Michael Kasha. After research fellowships at Harvard, Yale, and Caltech, he joined the faculty of the University of California, Los Angeles (UCLA), in 1961 and Georgia Tech in 1994. His current research includes the optical and electronic properties of nanomaterials and their applications in sensing, nanocatalysis, and nanomedicine.

ACKNOWLEDGMENTS

This material is based upon work supported by the National Science Foundation under Grant No. 1904351. The authors are grateful to Profs. Meilin Liu and Thomas Orlando for helpful scientific discussions and Cameron Ahmad, Luke Soule, and Abdulaziz Alabbady for their help and input.

REFERENCES

(1) Nazemi, M.; Panikkanvalappil, S. R.; El-Sayed, M. A. Enhancing the rate of electrochemical nitrogen reduction reaction for ammonia synthesis under ambient conditions using hollow gold nanocages. *Nano Energy* **2018**, *49*, 316–323.

(2) Nazemi, M.; El-Sayed, M. A. Plasmon-enhanced photo (electro) chemical nitrogen fixation under ambient conditions using visible light responsive hybrid hollow Au-Ag2O nanocages. *Nano Energy* **2019**, *63*, 103886.

(3) Nazemi, M.; Ou, P.; Alabbady, A.; Soule, L.; Liu, A.; Song, J.; Sulchek, T. A.; Liu, M.; El-Sayed, M. A. Electrosynthesis of Ammonia Using Porous Bimetallic Pd–Ag Nanocatalysts in Liquid-and Gas-Phase Systems. *ACS Catal.* **2020**, *10*, 10197–10206.

(4) Nazemi, M.; Panikkanvalappil, S. R.; Liao, C.-K.; Mahmoud, M. A.; El-Sayed, M. A. Role of Femtosecond Pulsed Laser-Induced Atomic Redistribution in Bimetallic Au–Pd Nanorods on Optoelectronic and Catalytic Properties. *ACS Nano* **2021**, *15*, 10241–10252.

(5) De Luna, P.; Hahn, C.; Higgins, D.; Jaffer, S. A.; Jaramillo, T. F.; Sargent, E. H. What would it take for renewably powered electrosynthesis to displace petrochemical processes? *Science* **2019**, *364*, No. eaav3506.

(6) Chen, J. G.; Crooks, R. M.; Seefeldt, L. C.; Bren, K. L.; Bullock, R. M.; Darensbourg, M. Y.; Holland, P. L.; Hoffman, B.; Janik, M. J.; Jones, A. K.; et al. Beyond fossil fuel−driven nitrogen transformations. *Science* **2018**, *360*, No. eaar6611.
(7) Lehnert, N.; Dong, H. T.; Harland, J. B.; Hunt, A. P.; White, C. J. Reversing nitrogen fixation. *Nat. Rev. Chem.* **2018**, *2*, 278−289.
(8) Smil, V. *Enriching the earth: Fritz Haber, Carl Bosch, and the transformation of world food production*; MIT press, 2004.
(9) Foster, S. L.; Bakovic, S. I. P.; Duda, R. D.; Maheshwari, S.; Milton, R. D.; Minteer, S. D.; Janik, M. J.; Renner, J. N.; Greenlee, L. F. Catalysts for nitrogen reduction to ammonia. *Nat. Catal* **2018**, *1*, 490−500.
(10) Spatzal, T.; Aksoyoglu, M.; Zhang, L.; Andrade, S. L.; Schleicher, E.; Weber, S.; Rees, D. C.; Einsle, O. Evidence for interstitial carbon in nitrogenase FeMo cofactor. *Science* **2011**, *334*, 940−940.
(11) Erisman, J. W.; Sutton, M. A.; Galloway, J.; Klimont, Z.; Winiwarter, W. How a century of ammonia synthesis changed the world. *Nat. Geosci.* **2008**, *1*, 636−639.
(12) Godfray, H. C. J.; Beddington, J. R.; Crute, I. R.; Haddad, L.; Lawrence, D.; Muir, J. F.; Pretty, J.; Robinson, S.; Thomas, S. M.; Toulmin, C. Food security: the challenge of feeding 9 billion people. *Science* **2010**, *327*, 812−818.
(13) Vojvodic, A.; Medford, A. J.; Studt, F.; Abild-Pedersen, F.; Khan, T. S.; Bligaard, T.; Nørskov, J. Exploring the limits: A low-pressure, low-temperature Haber−Bosch process. *Chem. Phys. Lett.* **2014**, *598*, 108−112.
(14) MacFarlane, D. R.; Cherepanov, P. V.; Choi, J.; Suryanto, B. H.; Hodgetts, R. Y.; Bakker, J. M.; Ferrero Vallana, F. M.; Simonov, A. N. A Roadmap to the Ammonia Economy. *Joule* **2020**, *4*, 1186−1205.
(15) Zamfirescu, C.; Dincer, I. Using ammonia as a sustainable fuel. *J. Power Sources* **2008**, *185*, 459−465.
(16) Klerke, A.; Christensen, C. H.; Nørskov, J. K.; Vegge, T. Ammonia for hydrogen storage: challenges and opportunities. *J. Mater. Chem.* **2008**, *18*, 2304−2310.
(17) Guo, W.; Zhang, K.; Liang, Z.; Zou, R.; Xu, Q. Electrochemical nitrogen fixation and utilization: theories, advanced catalyst materials and system design. *Chem. Soc. Rev.* **2019**, *48*, 5658−5716.
(18) Qiu, W.; Xie, X.-Y.; Qiu, J.; Fang, W.-H.; Liang, R.; Ren, X.; Ji, X.; Cui, G.; Asiri, A. M.; Cui, G.; Tang, Bo; Sun, X. High-performance artificial nitrogen fixation at ambient conditions using a metal-free electrocatalyst. *Nat. Commun.* **2018**, *9*, 3485.
(19) Gurudayal; Bullock, J.; Sranko, D. F.; Towle, C. M.; Lum, Y.; Hettick, M.; Scott, M. C.; Javey, A.; Ager, J. Efficient solar-driven electrochemical CO_2 reduction to hydrocarbons and oxygenates. *Energy Environ. Sci.* **2017**, *10*, 2222−2230.
(20) Schreier, M.; Héroguel, F.; Steier, L.; Ahmad, S.; Luterbacher, J. S.; Mayer, M. T.; Luo, J.; Grätzel, M. Solar conversion of CO_2 to CO using Earth-abundant electrocatalysts prepared by atomic layer modification of CuO. *Nat. Energy* **2017**, *2*, 17087.
(21) Bella, F.; Porcarelli, L.; Mantione, D.; Gerbaldi, C.; Barolo, C.; Grätzel, M.; Mecerreyes, D. J. C. s. A water-based and metal-free dye solar cell exceeding 7% efficiency using a cationic poly (3, 4-ethylenedioxythiophene) derivative. *Chem. Sci.* **2020**, *11*, 1485−1493.
(22) de Haro, J. C.; Tatsi, E.; Fagiolari, L.; Bonomo, M.; Barolo, C.; Turri, S.; Bella, F.; Griffini, G. J. A. S. C. Engineering. Lignin-Based Polymer Electrolyte Membranes for Sustainable Aqueous Dye-Sensitized Solar Cells. *ACS Sustainable Chem. Eng.* **2021**, *9*, 8550−8560.
(23) Tsuneto, A.; Kudo, A.; Sakata, T. Lithium-mediated electrochemical reduction of high pressure N_2 to NH_3. *J. Electroanal. Chem.* **1994**, *367*, 183−188.
(24) Lazouski, N.; Chung, M.; Williams, K.; Gala, M. L.; Manthiram, K. Non-aqueous gas diffusion electrodes for rapid ammonia synthesis from nitrogen and water-splitting-derived hydrogen. *Nat. Catal* **2020**, *3*, 463−469.
(25) Suryanto, B. H.; Matuszek, K.; Choi, J.; Hodgetts, R. Y.; Du, H.-L.; Bakker, J. M.; Kang, C. S.; Cherepanov, P. V.; Simonov, A. N.; MacFarlane, D. R. Nitrogen reduction to ammonia at high efficiency and rates based on a phosphonium proton shuttle. *Science* **2021**, *372*, 1187−1191.
(26) Carreon, M. L. Plasma catalytic ammonia synthesis: state of the art and future directions. *J. Phys. D: Appl. Phys.* **2019**, *52*, 483001.
(27) Hawtof, R.; Ghosh, S.; Guarr, E.; Xu, C.; Mohan Sankaran, R.; Renner, J. N. Catalyst-free, highly selective synthesis of ammonia from nitrogen and water by a plasma electrolytic system. *Science advances* **2019**, *5*, No. eaat5778.
(28) Rieger, P. H. *Electrochemistry*; Springer Netherlands, 1994.
(29) Fang, W.; Du, C.; Kuang, M.; Chen, M.; Huang, W.; Ren, H.; Xu, J.; Feldhoff, A.; Yan, Q. Boosting efficient ambient nitrogen oxidation by a well-dispersed Pd on MXene electrocatalyst. *Chem. Commun.* **2020**, *56*, 5779−5782.
(30) Greenlee, L. F. Recycling fertilizer. *Nat. Energy* **2020**, *5*, 557−558.
(31) Chen, G.-F.; Yuan, Y.; Jiang, H.; Ren, S.-Y.; Ding, L.-X.; Ma, L.; Wu, T.; Lu, J.; Wang, H. Electrochemical reduction of nitrate to ammonia via direct eight-electron transfer using a copper−molecular solid catalyst. *Nat. Energy* **2020**, *5*, 605−613.
(32) Wu, Z.-Y.; Karamad, M.; Yong, X.; Huang, Q.; Cullen, D. A.; Zhu, P.; Xia, C.; Xiao, Q.; Shakouri, M.; Chen, F.-Y.; et al. Electrochemical ammonia synthesis via nitrate reduction on Fe single atom catalyst. *Nat. Commun.* **2021**, *12*, 2870.
(33) Ahmadi, T. S.; Wang, Z. L.; Green, T. C.; Henglein, A.; El-Sayed, M. A. Shape-controlled synthesis of colloidal platinum nanoparticles. *Science* **1996**, *272*, 1924−1925.
(34) Sun, Y.; Xia, Y. Shape-controlled synthesis of gold and silver nanoparticles. *Science* **2002**, *298*, 2176−2179.
(35) Mahmoud, M.; Saira, F.; El-Sayed, M. Experimental evidence for the nanocage effect in catalysis with hollow nanoparticles. *Nano Lett.* **2010**, *10*, 3764−3769.
(36) Nazemi, M.; El-Sayed, M. A. Electrochemical Synthesis of Ammonia from N_2 and H_2O under Ambient Conditions Using Pore-Size-Controlled Hollow Gold Nanocatalysts with Tunable Plasmonic Properties. *J. Phys. Chem. Lett.* **2018**, *9*, 5160−5166.
(37) Nazemi, M.; El-Sayed, M. A. The Role of Oxidation of Silver in Bimetallic Gold−Silver Nanocages on Electrocatalytic Activity of Nitrogen Reduction Reaction. *J. Phys. Chem. C* **2019**, *123*, 11422−11427.
(38) Swearer, D. F.; Zhao, H.; Zhou, L.; Zhang, C.; Robatjazi, H.; Martirez, J. M. P.; Krauter, C. M.; Yazdi, S.; McClain, M. J.; Ringe, E.; et al. Heterometallic antenna- reactor complexes for photocatalysis. *Proc. Natl. Acad. Sci. U. S. A.* **2016**, *113*, 8916−8920.
(39) Wilson, A. J.; Mohan, V.; Jain, P. K. Mechanistic understanding of plasmon-enhanced electrochemistry. *J. Phys. Chem. C* **2019**, *123*, 29360−29369.
(40) Wilson, A. J.; Jain, P. K. Light-induced voltages in catalysis by plasmonic nanostructures. *Acc. Chem. Res.* **2020**, *53*, 1773−1781.
(41) Yan, Z.; Ji, M.; Xia, J.; Zhu, H. Recent Advanced Materials for Electrochemical and Photoelectrochemical Synthesis of Ammonia from Dinitrogen: One Step Closer to a Sustainable Energy Future. *Adv. Energy Mater.* **2020**, *10*, 1902020.
(42) Andersen, S. Z.; Čolić, V.; Yang, S.; Schwalbe, J. A.; Nielander, A. C.; McEnaney, J. M.; Enemark-Rasmussen, K.; Baker, J. G.; Singh, A. R.; Rohr, B. A.; et al. A rigorous electrochemical ammonia synthesis protocol with quantitative isotope measurements. *Nature* **2019**, *570*, 504−508.
(43) Suryanto, B. H.; Du, H.-L.; Wang, D.; Chen, J.; Simonov, A. N.; MacFarlane, D. R. Challenges and prospects in the catalysis of electroreduction of nitrogen to ammonia. *Nat. Catal* **2019**, *2*, 290−296.
(44) Greenlee, L. F.; Renner, J. N.; Foster, S. L. The use of controls for consistent and accurate measurements of electrocatalytic ammonia synthesis from dinitrogen. *ACS Catal.* **2018**, *8*, 7820−7827.
(45) Yang, X.; Nash, J.; Anibal, J.; Dunwell, M.; Kattel, S.; Stavitski, E.; Attenkofer, K.; Chen, J. G.; Yan, Y.; Xu, B. Mechanistic insights into electrochemical nitrogen reduction reaction on vanadium nitride nanoparticles. *J. Am. Chem. Soc.* **2018**, *140*, 13387−13391.
(46) Weng, L.-C.; Bell, A. T.; Weber, A. Z. Towards membrane-electrode assembly systems for CO 2 reduction: a modeling study. *Energy Environ. Sci.* **2019**, *12*, 1950−1968.

https://doi.org/10.1021/acs.accounts.1c00446
Acc. Chem. Res. 2021, 54, 4294−4304

(47) Ali, M.; Zhou, F.; Chen, K.; Kotzur, C.; Xiao, C.; Bourgeois, L.; Zhang, X.; MacFarlane, D. R. Nanostructured photoelectrochemical solar cell for nitrogen reduction using plasmon-enhanced black silicon. *Nat. Commun.* **2016**, *7*, 11335.
(48) Oshikiri, T.; Ueno, K.; Misawa, H. Plasmon□induced ammonia synthesis through nitrogen photofixation with visible light irradiation. *Angew. Chem.* **2014**, *126*, 9960−9963.
(49) González-Rubio, G.; Díaz-Núñez, P.; Rivera, A.; Prada, A.; Tardajos, G.; González-Izquierdo, J.; Bañares, L.; Llombart, P.; Macdowell, L. G.; Palafox, M. A.; et al. Femtosecond laser reshaping yields gold nanorods with ultranarrow surface plasmon resonances. *Science* **2017**, *358*, 640−644.
(50) Huang, W.; Qian, W.; El-Sayed, M. A. Photothermal reshaping of prismatic Au nanoparticles in periodic monolayer arrays by femtosecond laser pulses. *J. Appl. Phys.* **2005**, *98*, 114301.
(51) Grzelczak, M.; Perez-Juste, J.; García de Abajo, F. J.; Liz-Marzán, L. M. Optical properties of platinum-coated gold nanorods. *J. Phys. Chem. C* **2007**, *111*, 6183−6188.
(52) Plech, A.; Kotaidis, V.; Lorenc, M.; Boneberg, J. Femtosecond laser near-field ablation from gold nanoparticles. *Nat. Phys.* **2006**, *2*, 44−47.
(53) Minutella, E.; Schulz, F.; Lange, H. Excitation-dependence of plasmon-induced hot electrons in gold nanoparticles. *J. Phys. Chem. Lett.* **2017**, *8*, 4925−4929.
(54) Zandi, O.; Hamann, T. W. Determination of photoelectrochemical water oxidation intermediates on haematite electrode surfaces using operando infrared spectroscopy. *Nat. Chem.* **2016**, *8*, 778−783.
(55) Nazemi, M.; Soule, L.; Liu, M.; El-Sayed, M. A. Ambient Ammonia Electrosynthesis from Nitrogen and Water by Incorporating Palladium in Bimetallic Gold−Silver Nanocages. *J. Electrochem. Soc.* **2020**, *167*, 054511.
(56) Deng, Y.; Yeo, B. S. Characterization of electrocatalytic water splitting and CO_2 reduction reactions using in situ/operando Raman spectroscopy. *ACS Catal.* **2017**, *7*, 7873−7889.
(57) Jiao, F.; Xu, B. J. A. M. Electrochemical ammonia synthesis and ammonia fuel cells. *Adv. Mater.* **2019**, *31*, 1805173.

https://doi.org/10.1021/acs.accounts.1c00446
Acc. Chem. Res. 2021, 54, 4294−4304